Column chromatography for separation and fractionation of flavor-active esters on hydrophobic resins and simulation of breakthrough behavior

Saffarionpour, Shima; de Jong, Tessa F.; Van der Wielen, Luuk A.M.; Brouwer, Eric; Ottens, Marcel

DOI
10.1016/j.seppur.2018.05.008

Publication date
2019

Document Version
Final published version

Published in
Separation and Purification Technology

Citation (APA)
Saffarionpour, S., de Jong, T. F., Van der Wielen, L. A. M., Brouwer, E., & Ottens, M. (2019). Column chromatography for separation and fractionation of flavor-active esters on hydrophobic resins and simulation of breakthrough behavior. *Separation and Purification Technology*, *210*, 304-319. https://doi.org/10.1016/j.seppur.2018.05.008

Separation and Purification Technology 210 (2019) 304–319

Contents lists available at ScienceDirect

Separation and Purification Technology

journal homepage: www.elsevier.com/locate/seppur

Column chromatography for separation and fractionation of flavor-active esters on hydrophobic resins and simulation of breakthrough behavior

Shima Saffarionpour[a], Tessa F. de Jong[a], Luuk A.M. Van der Wielen[a,1], Eric Brouwer[b], Marcel Ottens[a,*]

[a] Delft University of Technology, Department of Biotechnology, Van der Maasweg 9, 2629 HZ Delft, The Netherlands
[b] Heineken Supply Chain, Burgemeester Smeetsweg 1, 2382 PH, Zoeterwoude, The Netherlands

ARTICLE INFO

Keywords:
Flavor-active esters
Adsorption
Frontal analysis
Fractionation
Simulation

ABSTRACT

For simulating an adsorption/elution step for separation and recovery of flavor-active esters in beer in the presence of ethanol at various temperatures, and validating the predicted breakthrough behavior, equilibrium data on concentration of each ester is required. This work evaluates the application of frontal analysis method (FA) for prediction of breakthrough behavior for adsorption of ethyl acetate, and determination of equilibrium concentrations and binding capacity for competitive adsorption of four major flavor-active esters in beer (i.e. ethyl acetate, isopentyl acetate, ethyl 4-methylpentanoate, and ethyl hexanoate), together with improvement of the obtained results, through fraction collection, and offline analysis, on columns packed with hydrophobic resins, Amberlite XAD16N and Sepabeads SP20SS. Single-component adsorption of ethyl acetate reveals a shorter breakthrough time, and higher slope of breakthrough curve for adsorption on SP20SS, due to smaller particle size, (50–100 μm), and enhanced mass transfer characteristics of this resin. Competitive frontal analysis tests, neatly demonstrate that increase in temperature is not favorable for adsorption but aids the elution step, 63–100% recovery of flavors at 333.15 K in comparison to 40–80% recovery at 298.15 K. Lower binding capacity of esters and shorter adsorption/elution cycle time is achieved at higher ethanol concentration and cyclic operation simulated under non-isothermal condition, exhibit higher accuracy between predicted and experimental breakthrough curves for XAD16N. A cyclic operation is simulated, for a larger scale column, for two scenarios, separation of ethyl acetate and complete separation of all flavor-active esters in the mixture. For more detailed prediction of breakthrough behavior, the influence of other components present in process streams needs to be investigated on competitive adsorption of esters.

1. Introduction

Liquid chromatography plays a key role in food industry nowadays which permits selective removal of wide variety of flavor and non-flavor-active food ingredients through adsorption [1–3]. In order to be able to design a process for separation and recovery of these ingredients, detailed knowledge on process conditions and their influence on adsorption is required. This implies that the adsorption equilibrium concentrations of each component in liquid-solid phase needs to be measured and well-understood. Among these components and ingredients, flavor-active esters play a major role in beverage and brewing industry, and are important contributors to the aroma profile of the beer product [4–9]. During processing, the level of these compounds might alter due to chemical and physical changes of the aroma complex. Their separation and fractionation can be challenging, since they are present in trace levels (ppm) with relatively large amounts of ethanol, which is present in process streams at higher concentration in comparison. To produce a final product with balanced flavor profile, which is acceptable by the consumer, controlling and adjusting the level of esters is crucial [4,10]. In order to design an adsorption process for selective recovery and fractionation of esters, multi-component thermodynamic adsorption equilibrium data and the influence of process conditions such as ethanol concentration and temperature on adsorption of flavor-active esters is required. For determination of competitive equilibrium condition, several chromatographic methods can be applied, among which dynamic methods proved to be the fastest and most accurate methods [11–13]. The best-known and widely adopted method is frontal analysis (FA), which allows measuring the mass of the

* Corresponding author.
E-mail address: m.ottens@tudelft.nl (M. Ottens).
[1] Bernal Institute, University of Limerick, Limerick, Ireland.

https://doi.org/10.1016/j.seppur.2018.05.008
Received 26 January 2018; Received in revised form 5 April 2018; Accepted 6 May 2018
Available online 17 May 2018

Nomenclature

A	cross-sectional area normal to flow direction (m^2)
C	concentration of analyte in bulk liquid (kmol/m^3)
C^*	concentration of analyte in liquid at equilibrium with stationary phase (kmol/m^3)
$C_{p,m}$	heat capacity of mobile phase (J/kg/K)
$C_{p,s}$	heat capacity stationary phase (J/kg/K)
C_0	effluent concentration (mg/ml)
C_{out}	concentration in outlet stream (mg/ml)
D_{app}	apparent dispersion coefficient (m^2/s)
D_{ax}	axial dispersion coefficient (m^2/s)
$D_{A,B}$	molecular diffusivity (m^2/s)
D_{eff}	effective diffusivity (m^2/s)
d_c	column diameter (m)
d_p	average adsorbent particle diameter (m)
d_{32}	Sauter mean diameter (m)
F	phase ratio (-)
ΔH	heat of adsorption (kJ/mol)
h_w	overall heat transfer coefficient at column wall (W/(m^2*K))
HTC	overall heat transfer coefficient between stationary and mobile phase (W/(m^2*K))
k_{eff}	effective mass transfer coefficient (m^2/s)
$\tilde{k}'$	modified retention factor (-)
k'	retention factor (-)
k_{ads}	Langmuir constant (m^3/kmol)
K	permeability of medium (m^2)
k_{ov}	overall mass transfer coefficient (1/s)
k_f	external mass transfer coefficient (m/s)
L	column length (m)
M_B	molecular weight of solvent (g/mol)
m_{resin}	mass of resin (g)
N	Avogadro's constant (mol^{-1})
q_{max}	maximum load (kmol/kg_{resin})
Q_f	volumetric flow-rate (m^3/s)
q	concentration of analyte in stationary phase (kmol/kg_{resin})
q_{EBC}	equilibrium binding capacity (mg)
r_m	molecular radius (m)
S_v	surface-face-to-volume ratio of packing material (m^2/m^3)
SASA	solvent accessible surface area (m^2)
t	time (s)
$t_{R,i}$	retention time of component i (s)
t_0	dead time of the column (for total liquid holdup) (s)
T_m	absolute temperature of mobile phase (K)
T_s	absolute temperature stationary phase (K)
T_w	absolute temperature column wall (K)
t_b	breakthrough time (s)
u	linear velocity of mobile phase (m/s)
u_{int}	interstitial velocity (m/s)
u_{int}	interstitial velocity (m/s)
V_c	column volume (ml)
V_A	molar volume (cm^3/mol)
V_{int}	interstitial volume (ml)
V_a	breakthrough volume for adsorption (ml)
V_h	holdup volume (ml)
V_d	desorbed volume (ml)
V_{init}	initial volume (ml)

Greek symbols

ε_T	total porosity (-)
λ_L	axial thermal conductivity (W/(m*K))
λ_S	thermal conductivity of stationary phase (W/(m*K))
ρ_p	density of adsorbent (kg/m^3)
ρ_L	density of mobile fluid (kg/m^3)
ν	kinematic viscosity (m^2/s)
ε	column void fraction (-)
ε_p	particle porosity (-)
ε_{bed}	average bulk porosity of packed bed (-)
Φ	sphericity of adsorbent (-)
η_B	solvent viscosity (cP)
ψ_B	constant for solute-solvent interaction (-)
τ_p	Tortuosity factor (-)
ψ_p	diffusional hindrance factor (-)
λ_m	ratio between radius of molecule and pore radius (-)

adsorbed component at equilibrium from the retention time of the breakthrough front. As one of the variants of this method, staircase frontal analysis is well-suited for measurement of the concentrations in intermediate sub-plateaus for a multi-component mixture [14–16]. However, for a mixture consisting of components with similar molecular structure, physical properties, and similar retention times, this method cannot merely be used for estimation of equilibrium concentration for each component in the mixture, as more than one component might be detected in one sub-plateau. To improve and overcome this problem, the competitive frontal analysis method can be combined with fraction collection and offline analysis, to measure the concentration of each component present in the mixture and in each sub-plateau of the breakthrough front. This work aims to investigate the application of the competitive frontal analysis method for measurement of the equilibrium adsorption for a multi-component mixture of major esters present in a beer matrix, i.e. ethyl acetate, isopentyl acetate, ethyl 4-methylpentanoate, and ethyl hexanoate and study the possibility of their separation in a fixed-bed column through simulation of breakthrough behavior. In order to investigate the possibility for separation of these flavor-active esters, and study the influence of temperature and ethanol concentration on their competitive adsorption behavior, competitive frontal analysis method is applied in combination with fraction collection via the outlet stream and offline analysis to determine the concentration associated with each ester present in each intermediate sub-plateau. The equilibrium binding capacity is estimated for each ester present in the mixture from retention time and the breakthrough front, also from the breakthrough curves constructed through fraction collection. Possibility for separation of the aforementioned flavor-active esters, is investigated on columns packed with Amberlite XAD16N and Sepabeads SP20SS resins, which showed high selectivity towards esters in our previous studies [8,17]; also similar resins with the styrene- divinylbenzene structure showed potential for separation and recovery of phenolic components as is demonstrated in many research works reported in the literature, both for batch and fixed bed operations [18–20]. Additionally, breakthrough behavior is simulated and predicted in Aspen Adsorption V8.8, considering the equilibrium dispersive chromatographic model, for separation of the esters under the conditions tested at lab-scale and the results of the simulations are compared with experimental validation tests. The influence of the flowrate and column length is demonstrated on shape and breakthrough retention time for adsorption on both resins for adsorption of ethyl acetate and the observed breakthrough behavior is explained based on properties for each tested adsorbent. The required parameters for simulation, i.e. single and multi-compound adsorption parameters for adsorption of esters based on the Langmuir isotherm model and heat of adsorption of the individual components, obtained through single-component isotherm studies at different temperatures and Van't Hoff relation, are acquired from previous work [8,17], and used as input for

simulation. Based on the lab-scale tests, a similar condition is simulated for a larger scale fixed-bed column for cyclic operation and separation of flavor-active esters. Two different scenarios are simulated, for separation of ethyl acetate as the major ester present in beer and separation of all of the flavor-active esters from the feed stream. For the simulated scenarios, the percentage of recovery for each tested ester and the productivity, the amount of feed processed during each batch cycle time, are calculated. This simulation can be applied and adapted to study the possibility for separation of mixture of other components on a column packed with the same hydrophobic resins, knowing the required parameters for simulation, i.e. multicomponent isotherm parameters and values for heat of adsorption for each individual component present in the mixture.

2. Materials and methods

2.1. Materials

2.1.1. Chemicals

Ethyl acetate (purity ≥ 99.5%), isopentyl acetate (98%), ethyl hexanoate, and ethyl 4-methylpentanoate are purchased from Sigma-Aldrich. MilliQ water is used for dilutions and ethanol 96%, is purchased from Merck. The tested flavor-active esters with their main physical properties are presented in Appendix A, Table A2.

2.1.2. Adsorbents

Food grade resin XAD16N from Amberlite resin series and the aromatic type Sepabeads SP20SS from HP resin series are purchased from Sigma-Aldrich and used for adsorption tests. Detailed specifications and physical properties of the tested resins are reported in Appendix A, Table A1 [21].

2.2. Methods

2.2.1. Chromatographic model

2.2.1.1. Equilibrium dispersive model (EDM). The equilibrium dispersive model, proposed by Lapidus and Amundson [22], proved to be successful in considering contributions leading to band broadening effects, such as axial dispersion and rate of mass transfer. The first equation of this model related to mass balance can be written as Eq. (1) [11,12,22–27].

$$\frac{\partial C_i}{\partial t} + F\frac{\partial q_i}{\partial t} + \frac{\partial (uC_i)}{\partial z} = \widetilde{D}_{app,i}\frac{\partial^2 C_i}{\partial z^2} \tag{1}$$

F is the phase ratio ($F = V_s/V_m = (1 - \varepsilon_T)/\varepsilon_T$), and parameter $\widetilde{D}_{app,i}$ expresses the apparent dispersion coefficient including also the volume fractions and has relation with $D_{app,i}$ and axial dispersion coefficient (D_{ax}), as is explained in Appendix B, Eqs. (B.1) and (B.3) [26]. The second equation for equilibrium dispersive model, relates the two concentrations in Eq. (1), based on a linear kinetic model, presented as Eq. (2) [12,25].

$$\frac{\partial q_i}{\partial t} = k_{ov}(C_i - C_i^*) \tag{2}$$

By knowing the adsorption isotherms, elution profiles and breakthrough curves can be predicted. The extension of the Langmuir model, which describes the competition of component i with nc components in the mixture, is used, explained as Eq. (3) [12,17,28–32].

$$q_i = \frac{q_{max} k_{ads,i} C_i}{1 + \sum_{j=1}^{nc} k_{ads,j} C_j} \tag{3}$$

An adsorption column is simulated, considering two different constant states [33]. As initial condition:

$$c_i(t = 0, x) = c_i^{Init};\ i = 1, \cdots, N \tag{4}$$

In addition, boundary condition:

$$c_i(t, x = 0) = c_i^{Feed} \tag{5}$$

The contribution of axial dispersion, D_{ax} (m^2/s), and rates of mass transfer, k_{ov} (m^2/s), can be estimated theoretically based on relations proposed in the literature, explained in the sections related to estimation of model parameters.

2.2.1.2. Non-isothermal adsorption system. In order to consider the heat of adsorption and deviation of the system from isothermal behavior, two differential energy balance equations are considered to complete the set of partial differential equations [12,34], for the mobile and stationary phases. For the non-isothermal system, the differential energy balance for mobile phase can be written as Eq. (6).

$$-\lambda_L \varepsilon \frac{\partial^2 T_m}{\partial z^2} + C_{p,m}\rho_m u\frac{\partial T_m}{\partial z} + \varepsilon\, C_{p,m}\rho_m \frac{\partial T_m}{\partial t} + +S_v(1-\varepsilon)HTC(T_m - T_s) + \frac{4h_w}{d_c}(T_m - T_w) = 0 \tag{6}$$

Moreover, energy balance for stationary phase can be presented as:

$$-\lambda_s \frac{\partial^2 T_s}{\partial z^2} + \rho_p C_{p,s}\frac{\partial T_s}{\partial t} + \rho_p \frac{\partial T_s}{\partial t}\sum_{i=1}^{nc}(C_{p,m}q_i) + \rho_p \sum_{i=1}^{nc}(\Delta H_i \frac{\partial q_i}{\partial t}) - S_v HTC(T_m - T_s) = 0 \tag{7}$$

Here the system is considered as adiabatic with fluid and solid phase conduction.

2.2.2. Estimation of model parameters

2.2.2.1. Axial dispersion coefficient. Axial Dispersion (D_{ax}) is estimated based on a dimensionless equation, proposed by Chung and Wen (1968) and Wen and Fan (1975). This equation shows dependency of the dispersion coefficient on the particle Reynolds number as presented in Eq. (8) [26].

$$D_{ax} = \frac{u_{int} d_p \varepsilon}{0.2 + 0.011(\varepsilon\, Re)^{0.48}} (10^{-3} \le Re \le 10^3) \tag{8}$$

where ($u_{int}\, d_p/D_{ax}$) is known as the Peclet (Pe) number, and Re = ($u_{int}\, d_p/\nu$).

2.2.2.2. Pressure drop. A linear relation is normally considered between flow-rate and pressure drop explained based on Darcy's law, for (Re < 10) and steady state condition [4,35] as is explained in Eq. (9).

$$Q_f = \frac{KA}{\mu L}\Delta P \tag{9}$$

Assuming that the granular bed is analogues to a group of capillaries, parallel to the direction of flow, the permeability term (K) of the medium can be written as presented in Eq. (10).

$$K = \frac{\varepsilon_{bed}{}^3}{2\tau_p{}^2 S_v^2 (1-\varepsilon_{bed})^2} \tag{10}$$

The value of τ_p, tortuosity of the bed, is defined as the ratio of the actual tortuous length traveled by the fluid in the bed to the geometrical length of the bed. If the packing material is formed by mono-sized spheres, the term S_v can be simplified to $S_v = 6/d_p$ and $\tau_p = 1.58$; Eq. (9) can then be reduced to the Kozeny-Carman relation as expressed in Eq. (11) [13,35–39].

$$K = \frac{\varepsilon_{bed}{}^3 d_p^2}{180(1-\varepsilon_{bed})^2} \tag{11}$$

where d_p is the diameter of the packing sphere and 180 is the Kozeny-Carman pre-factor [36]. If the packing material is non-spherical and shows a distribution in size, it should be taken into account and $d_p = \Phi\, d_{32}$. In case of having spherical packing material, the value of Φ will be equal to one.

2.2.2.3. Overall mass transfer coefficient. The overall mass transfer coefficient is estimated based on Eq. (12), which can be described as [34,37]:

$$k_{ov} = \left[\frac{d_p}{6k_f} + \frac{d_p^2}{60\varepsilon_p D_{eff}}\right]^{-1} \tag{12}$$

The external mass transfer coefficient k_f is estimated based on Wilson and Geankoplis correlation, as is described in Eqs. (13) and (14) [40,41].

$$Sh = \frac{1.09}{\varepsilon} Re^{1/3}\, Sc^{1/3};\ 0.0015 < Re < 55 \tag{13}$$

$$Sh = \frac{d_p k_f}{D_{AB}};\ Re = \frac{u_{int} d_p}{\nu};\ Sc = \frac{\nu}{D_{AB}} \tag{14}$$

The free molecular diffusivity of moderate molecular weight compound, (D_{AB}) (molecular weight between 100 and 500) can be estimated as proposed by Wilke and Chang, described in Eq. (15) [12,40,42]. This relation is the most popular relation for the molecular diffusivities of low molecular weight compounds in conventional solvents.

$$D_{A,B} = 7.4 \times 10^{-8} \frac{\sqrt{\psi_B M_B}}{\eta_B V_A^{0.6}} T \tag{15}$$

The value of ψ_B, which counts for solute-solvent interactions, is equal to 1 for all non- associated solvents and recommended as 2.6 for water [12,42]. The value for molar volume is estimated based on molecular radius (r_m) as described by Eq. (16) [43].

$$V_A = 4\pi r_m^3 N/3 \tag{16}$$

Molar radius is calculated based on solvent accessible surface area (*SASA*) [44], which considering a spherical surface area, it is then possible to calculate the molar radius from Eq. (17) [43].

$$r_m = \sqrt{\frac{SASA}{4\pi}} \tag{17}$$

The effective diffusivity considers corrections in free molecular diffusivity D_{AB}, by taking into account the effect of diffusional hindrance factor ψ_p, the intraparticle porosity (ε_p) and the tortuosity factor τ_p [45], which for randomly oriented cylindrical pores, may be considered equal to 3 [34]. The relation for effective diffusivity can be presented as shown in Eq. (18) [46,47].

$$D_{eff} = \frac{\varepsilon_p D_{AB}}{\tau_p} \psi_p \tag{18}$$

In order to estimate the diffusional hindrance factor ψ_p, the ratio between the radius of the molecule (r_m) and radius of the adsorbent pore (r_{pore}), which is explained by λ_m needs to be determined.

For $\lambda_m < 2$ the diffusional hindrance factor can be calculated using Eq. (19) [45].

$$\psi_p = 1 + \frac{9}{8}\lambda_m \ln(\lambda_m) - 1.539\lambda_m \tag{19}$$

With the estimation of diffusivities and the overall mass transfer coefficients, the required parameters will be obtained for simulating the condition in Aspen Adsorption.

2.2.3. Simulation in Aspen adsorption

Aspen Adsorption V8.8 is used as a simulation environment to design a liquid adsorption step for flavor-active esters, knowing the thermodynamic parameters and physical properties of the tested components and the adsorbent materials. More explanation on simulation environment of Aspen Adsorption and the assumptions considered for the simulation are provided in Appendix C.

2.2.4. Competitive frontal analysis

Various chromatographic methods are available for determination of adsorption isotherms, and equilibrium concentrations among which Frontal Analysis (FA) is widely applied in liquid chromatography [11,13,33,48,49]. This method has application in determination of equilibrium concentrations and single-solute isotherms, through concentration dependency of the retention times in breakthrough fronts, however for determination of equilibrium concentrations for a multi-compound mixture, the composition of components in the intermediate plateaus needs to be measured [33] and this method can be applied for calculation of equilibrium binding capacity and determination of equilibrium concentrations for a multicomponent mixture, only when clear breakthrough fronts can be detected for each component in the mixture. A sample breakthrough front for a multi-compound mixture, consisting of three components is illustrated in Appendix D, Fig. D.1. The adsorbed amount for each component and the amount of mass desorbed from the column can be calculated based on Eqs. (D.1)–(D.6), presented in Appendix D for the first, second, and the third component [48,50,51].

With the use of the discussed approach, the possibility for separation of four major hydrophobic flavor-active esters in beer is tested in a packed column and the application of competitive frontal analysis is evaluated for calculation of equilibrium concentrations and binding capacity. Since the molecular structure and physical properties of the two tested esters with the highest hydrophobicity is similar, separate breakthrough curves could not be detected for these two components, as they are detected in one sub-plateau and this method could not be successfully applied for determination of equilibrium binding capacity and for more accurate measurement of the composition corresponding to each ester, fractions are collected and analyzed through offline analysis. Through these measurements, breakthrough curves can be constructed during the sampling time and at the tested column volume. The concentration of the compound of interest in the stationary phase, q, can then be determined through integration of the constructed breakthrough curves, which is known as the Equilibrium Binding Capacity (q_{EBC}) (mg), and can be obtained by integrating the area above the breakthrough curves, considering the dead volume for the system [17,49,52], according to Eq. (20).

$$q_{EBC,i} = \int_0^{V_c} (C_{0,i} - C_{out,i}) dV_c \ \mathrm{i} = 1, \ldots, \mathrm{N} \tag{20}$$

The equilibrium binding capacity per gram of the adsorbent can then be calculated for each component from Eq. (21).

$$q_{e,i} = \frac{q_{EBC,i}}{m_{resin}} \tag{21}$$

The influence of ethanol and temperature is investigated on breakthrough fronts, the constructed breakthrough curves through fraction collection, and subsequently the estimated binding capacity and for the prediction of breakthrough behavior, the adsorption parameters acquired from our previous studies [8] on batch uptake experimentation are used as input parameters for the simulation. The obtained breakthrough fronts and the constructed breakthrough curves derived from fraction collection, are used to validate the results of the simulation.

2.2.5. Error estimation

The error between the predicted values of C/C_0 obtained from simulation and the experimental breakthrough curves constructed through fraction collection and offline analysis, are estimated with Marquardt's percent standard deviation (*MPSD*), as presented in Eq. (22) [53].

$$MPSD = 100\sqrt{\frac{1}{N-P}\sum_{i=1}^{N}\left[\frac{(C/C_0)_{exp} - (C/C_0)_{cal}}{(C/C_0)_{exp}}\right]_i^2} \tag{22}$$

where N is the number of data points and P is the degrees of freedom. Also the percent deviation between the experimental and the breakthrough times derived from the simulation are calculated according to Eq. (23) [54].

$$E(t_b)\% = 100\left(\frac{t_{b,exp}-t_{b,cal}}{t_{b,exp}}\right) \quad (23)$$

3. Experimental

3.1. Chromatographic system

Frontal analysis is applied to obtain the breakthrough fronts and curves for determination of equilibrium concentrations. Experiments are carried out for single-solute mixture of 0.9 g/L of ethyl acetate prepared in 0.1% (v/v) co-solvent mixture of ethanol/water. The same background solution is used for elution steps. Tests are performed using columns packed with hydrophobic resins, Sepabeads SP20SS and Amberlite XAD16N, which showed high affinity towards esters in our previous studies [8,17]. Resins are packed in an Omnifit glass chromatography column, *ID* 15 mm, column length 150 mm (Thermofischer Scientific), suitable for experimental tests up to 40 bar. The experimental breakthrough data are processed using the UNICORN 5.1.1 data acquisition software. Multi-component breakthrough analysis is performed for a multi-component mixture of four major esters in beer (i.e. ethyl acetate, isopentyl acetate, ethyl 4-methylpentanoate and ethyl hexanoate), approximately 0.45 g/L of each component prepared in different concentrations of ethanol/water co-solvent mixture (i.e. 1 and 30% v/v) and at three different temperatures (i.e. 293.15, 313.15, and 333.15 K). Fractions are collected in Eppendorf conical tubes 15 ml (purchased from Eppendorf Netherlands B.V.), using fraction collector FRAC 920, and column tests are performed on Äkta Explorer system 100, both purchased from General Electric Life Sciences, Uppsala, Sweden.

3.2. Setup

The Äkta explorer 100, FPLC chromatography system, is used for the breakthrough analysis tests. Samples are pumped through Äkta explorer pump P-900 (General electric Life Sciences, Uppsala, Sweden) to the system through an eight-port column selection valve [35]. The effluent from the analytical column, was monitored by a UV 900 detector (General electric Life Sciences, Uppsala, Sweden). For the tests performed at elevated temperatures, the column is heated using a heated tubing around the column, pumping water through a Lauda heating circulator circulating water bath MT/M3 (purchased from Lauda-Brinkmann, USA).

3.3. Procedures

Single-component tests are performed for ethyl acetate solution and breakthrough curves are obtained for various tested flow-rates, and column lengths, mentioned in the previous section, both for a column packed with Sepabeads SP20SS resin and Amberlite XAD16N. The shape of the breakthrough curves and the retention times are compared for adsorption of this ester on both resins and the breakthrough curves are simulated under the same condition in Aspen Adsorption as explained in Section 2.2.3, and compared with the experimental breakthrough curves. Next, the possibility of separation for the four major mentioned flavor-active esters is investigated in a multi-compound mixture at various ethanol concentrations and temperatures, explained in Section 4.3. The column is preheated when tested at elevated temperatures. Stepwise breakthrough fronts are obtained for both adsorption and elution. Elution is performed with the same background co-solvent mixture of ethanol/water used for preparation of the initial sample solution. To measure the intermediate concentrations for each component in the sub-plateaus, 5 ml fractions are collected in 15 ml Eppendorf tubes from the outlet stream with the time interval of 2.5 min. Tubes are immediately closed after fraction collection and 5 ml of each selected fraction is added to 10 ml headspace vials and transferred to the GC for measurement. The collected fractions added to vials are subsequently analyzed using Static-Headspace-Gas-Chromatography (HS-GC) method with the GC (Trace 1300, Thermofischer Scientific, Switzerland) coupled with Triplus RSH Autosampler (Thermofischer Scientific, Switzerland) and FID in a RESTEK Rxi 624Sil MS column (20 mm × 0.18 mm *ID* × 1 μm *df*). Helium was selected as the carrier gas in the system. The agitator temperature was set to 40 °C and samples are measured with incubation time of 20 min. Syringe temperature was set to 60 °C and detector temperature to 250 °C. Split ratio of 30 was used for the measurements. Ramped oven temperature was considered for the GC settings, 60 °C with holding time of 1 min, increase to 75 °C with the speed of 10 °C/min, and the second increase to 175 °C with the speed of 30 °C/min with the holding time of 1 min. The retention time of tested components is measured during 7 min. The chromatograms obtained from the measurements show the retention time (minutes) of 1.5, 2.4, 4.9, 5.5, and 5.7 for ethanol, ethyl acetate, isopentyl acetate, ethyl 4-methylpentanoate, and ethyl hexanoate respectively. The breakthrough curves are constructed with the measured concentrations for each ester present in the mixture. The collected fractions and breakthrough curves are compared at various tested ethanol concentrations and temperatures.

4. Results and discussions

4.1. Estimated parameters

The required model parameters, explained in Sections 2.2.2 and 2.2.3, are estimated for each tested condition (i.e. tested resin, flowrate, column length, and initial feed concentration). The main considered physical properties and column conditions are assembled in Table 1.

In order to simulate the breakthrough behavior, in Aspen Adsorption, the required Langmuir parameters for single and multi-component adsorption, presented in Eq. (4), derived from batch uptake experimentation at various ethanol concentrations and temperatures and the values for heats of adsorption for each tested ester, are obtained from our previous studies, to consider the deviation of the system from isothermal behavior [8]. The values for heats of adsorption for each tested ester, and for adsorption on each tested resin are assembled in Appendix A, Table A3. The value of volumetric heat capacity for the synthetic adsorbents with the structure of Styrene-divinylbenzene, $C_{p,s}$ is considered as 1758.4 J/kg/K [42]. Specific heat of the mixtures

Table 1
Resin physical properties and column condition for the experimental tests and simulation.

	Resin	
Physical properties	Amberlite XAD16N	Sepabeads SP20SS
Resin particle diameter d_p (cm)	0.071	0.010
Resin density $\rho_{dry\ resin}$ (g/ml)	1.01	1.08
Resin density $\rho_{wet\ resin}$ (g/ml)	1.30	1.02
Column length L (cm)	1, 3, 5	1, 3, 5
Column diameter d_c (cm)	1.5	1.5
Feed flowrate Q_f (ml/min)	2, 5, 8	2, 5, 8, 10
Intraparticle porosity ε_p (-)	0.36	0.57
Total porosity ε_T (-)	0.55	0.79
Void fraction ε (-)	0.31	0.51
Adsorption temperature (K)	298.15, 333.15	298.15, 313.15, 333.15
Ethanol concentration %(v/v)	0.1, 1, 30	0.1, 1, 30
Initial feed concentration C_0 (g/L)	0.90, 0.45	0.90, 0.45

tested, considering the small molar fractions of the solutes in comparison to water is estimated as close to $C_{p,m}$ of water, estimated at various tested temperatures (e.g. $C_{p,m}$ at T = 298.15 K is estimated as 4179.7 J/Kg/K [55], and thermal conductivity of the mixture is estimated as 0.61 W/m/K [55]).

4.2. Single-component breakthrough simulation

Considering the assumptions, and required model parameters discussed in Section 4.1, the breakthrough behavior is simulated in Aspen Adsorption for single-component adsorption of ethyl acetate at various flowrates and column lengths, in order to study the accuracy and agreement of the model predictions with the experimental data. For the experimental tests adsorption of ethyl acetate is investigated on a 3 cm column packed with resins, Sepabeads SP20SS, and Amberlite XAD16N and at various flow-rates (i.e. 2, 5, and 8 ml/min), and for a flow-rate of 10 ml/min for various column lengths for Sepabeads SP20SS resin (i.e. 1, 3, and 5 cm) column, and a flow-rate of 2 ml/min for the same column lengths of Amberlite XAD16N.

4.2.1. Influence of flow-rate

The results of the simulation are compared with the experimental breakthrough curves, obtained from column breakthrough analysis tests, depicted in Fig. 1 for adsorption on Sepabeads SP20SS and Amberlite XAD16N respectively. As can be observed from Fig. 1, one adsorption/elution cycle for Sepabeads SP20SS resin takes approximately half the time in comparison to Amberlite XAD16N (e.g. 150 min for flow-rate of 2 ml/min in comparison to approximately 300 min on Amberlite XAD16N), and the breakthrough curves observed on Sepabeads SP20SS resin, show steeper slope. The reason for being able to achieve earlier breakthrough time and steeper breakthrough curve for adsorption on Sepabeads SP20SS resin, can be explained by the resin structure. This resin has smaller particle size (50–100 μm) in comparison to Amberlite XAD16N (250–710 μm), therefore it is possible to pack the Sepabeads SP20SS resin tighter in the column, which leads to less extra particle space (space between the particles), and less flow-through around the particles, since higher extra-particle space can cause the flow to follow the path with the least resistance [45], which occurs here for Amberlite XAD16N with larger particle diameter. Moreover, a smaller particle size of Sepabeads SP20SS resin and higher intraparticle porosity (ε_p) for this resin in comparison to XAD 16 N can lead to enhanced mass transfer and more effective diffusivity (D_{eff}) due to more intraparticle diffusion, explained by the inverse of the second term in Eq. (12), which is higher in comparison to external mass transfer coefficient (k_f) for SP20SS resin in comparison to XAD16N, [56], and leads to shorter mass transfer zone and a steeper breakthrough curve.

In contrast to breakthrough curves obtained for adsorption on Sepabeads SP20SS, the breakthrough curves for Amberlite XAD16N, demonstrate a different behavior, the breakthrough time is earlier and later exhaustion point is achieved on this resin, as the mass transfer zone is longer and more dispersed on this resin. Similar shape of the breakthrough curves obtained for adsorption on Sepabeads SP20SS indicates that even at higher flow-rates the residence time of ethyl acetate in the column was long enough for the mass transfer to occur. Different observed shape for the breakthrough curves for adsorption on XAD16N at higher flowrates in comparison to flowrate of 2 ml/min implies that more residence time for enhanced mass transfer characteristics is required for adsorption on this resin. The obtained results are in agreement with the results reported in the literature on studying the adsorption behavior of phenolic compounds on the resins with similar structure, i.e. XAD16HP and SP700, as external mass transfer is more dominant in the beginning of adsorption and early breakthrough behavior is observed at higher flow rates [19].

4.2.2. Influence of column length

The experimental breakthrough curves obtained at various tested column lengths are compared with Aspen simulations for adsorption on the two tested resins, presented in Fig. 2. The breakthrough curves obtained for adsorption of ethyl acetate on Sepabeads SP20SS resin show a proportional increase in the breakthrough time and no change in the shape of the breakthrough curve was observed when the column length was increased. An increase in bed length increases the mass transfer zone; therefore, there will be a longer distance from column

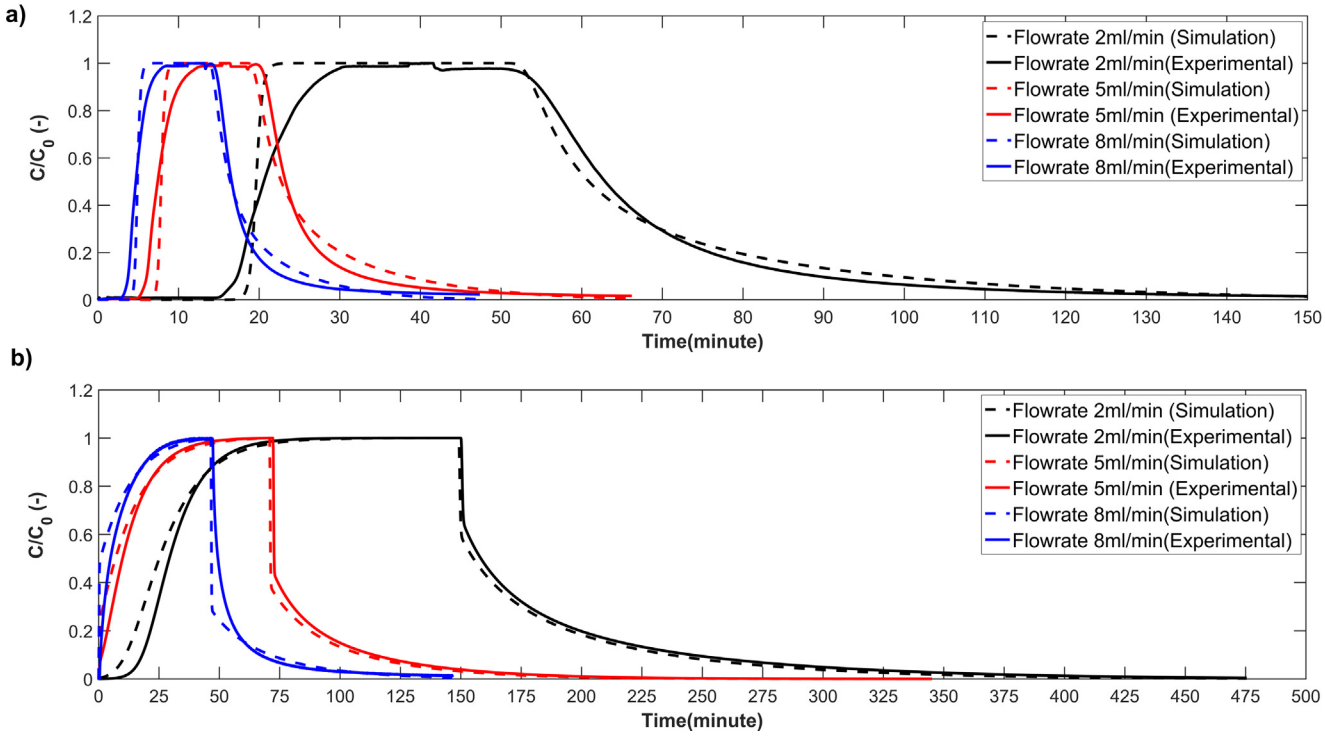

Fig. 1. Influence of flow-rate on single-component adsorption of ethyl acetate on a 3 cm column. (a) Sepabeads SP20SS, (b) Amberlite XAD16N.

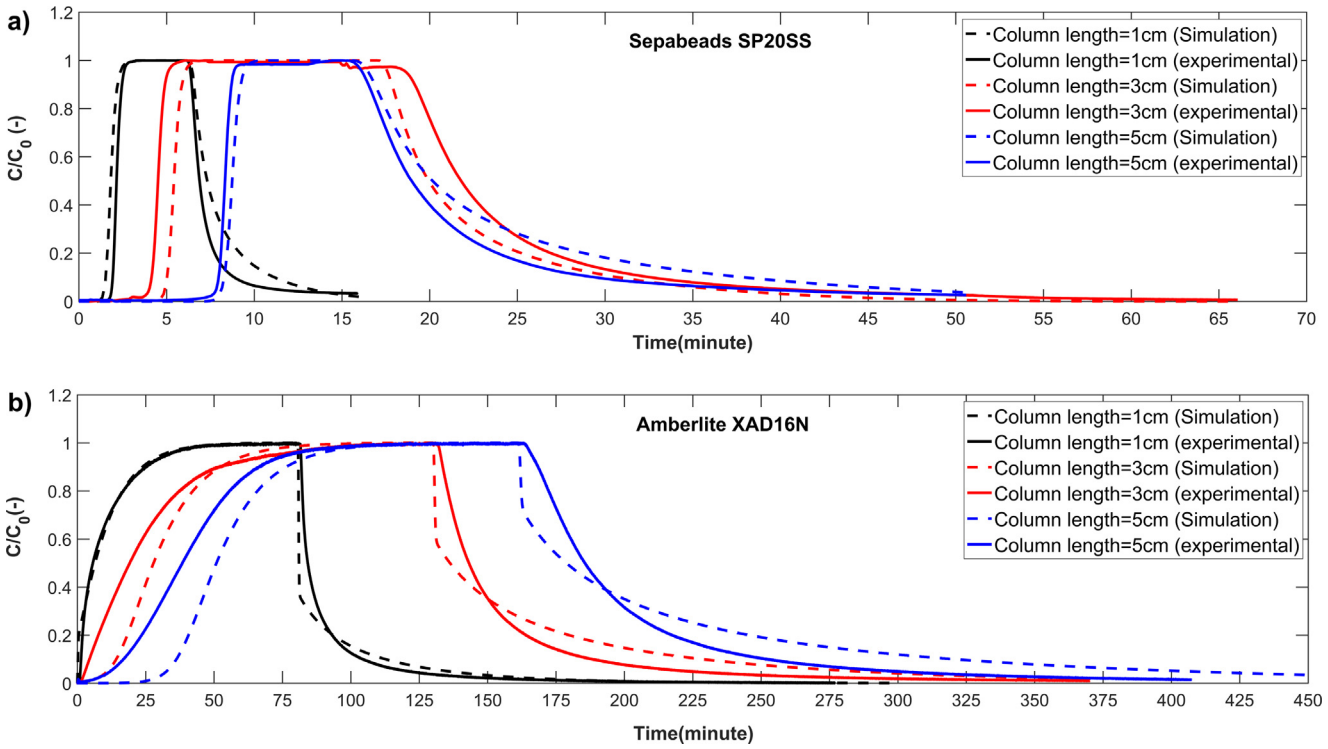

Fig. 2. Influence of bed length on single-component adsorption of ethyl acetate; (a) Sepabeads SP20SS (Flow-rate 10 ml/min) (b) Amberlite XAD16N (Flow-rate 2 ml/min).

entrance to the exit point, which results in an extended breakthrough time. While the breakthrough time increases proportionally for adsorption on Sepabeads SP20SS, for various tested column lengths, different behavior is observed for adsorption on Amberlite XAD16N, Fig. 2, *part b*; where the shape of the breakthrough curve observed as different when the tests are performed for a longer column (i.e. 5 cm here).

The observed phenomena can be explained by the shorter length of the used column, which has influence on pore diffusion. Due to the short column length used for Amberlite XAD16N (1 cm), pore diffusion is not sufficient which leads to earlier increase of effluent concentration and earlier breakthrough time. The estimated errors for the breakthrough curves presented in Figs. 1 and 2 are estimated as explained in Section 2.2.5, assembled in Table 2.

As can be concluded from the presented values in Table 2, predictions at various flowrates show a more accurate estimation in comparison to different tested column lengths. For the tests performed on the two tested resins, at different flowrates, higher accuracy and lower standard error is calculated for adsorption on XAD16N in comparison to SP20SS. In comparison to the tests performed at various flowrates, the results of the tests at different column lengths show a higher percent standard error, specifically for the tests performed on a 1 cm column packed with SP20SS, in which a larger deviation between simulation prediction and the experimental breakthrough front is observed in the elution step. For adsorption/elution on XAD16N, a higher standard deviation was obtained for adsorption on a 5 cm column in comparison to the other two tested lengths.

4.3. Multi-component breakthrough simulation

4.3.1. Influence of temperature

In order to investigate the influence of temperature on multi-component adsorption of flavor-active esters, competitive frontal breakthrough analysis is performed to test the multi-component separation of four major aforementioned flavor-active esters in beer. The influence of temperature is investigated both on the obtained breakthrough fronts and on the collected fractions. The comparison of the breakthrough curves with the collected fractions is depicted in Fig. 3 for each tested temperature.

The amount of equilibrium binding capacity is estimated for each ester present in the mixture and for the three tested temperatures, according to the procedure explained in Section 2.2.4 based on competitive frontal analysis and compared with the results obtained from integration of the breakthrough curves derived from fraction collection and offline analysis. The two components with higher hydrophobicity and similar molecular structure (i.e. ethyl 4-methylpentanoate and ethyl hexanoate) have the same physical properties and similar breakthrough time and show a similar breakthrough behavior and both are detected in the third sub-plateau of the competitive frontal curve, therefore for estimation of equilibrium binding capacity, based on the competitive frontal analysis, both are considered in the third sub-

Table 2
Estimated errors for breakthrough times and percent standard deviation between simulated breakthrough curves and experimental frontal curves; Adsorption at 298.15 K and initial solution prepared in 1% v/v Ethanol.

	Sepabeads SP20SS Flowrate (ml/min)			Amberlite XAD16N Flowrate (ml/min)		
	2 (ml/min)	5 (ml/min)	8 (ml/min)	2 (ml/min)	5 (ml/min)	8 (ml/min)
$E(t_b)$%	3.85	0.080.24		0.11	0	0.035
MPSD	55.69	23.50	90.12	26.48	35.05	33.23
	Column length (cm)			Column length (cm)		
	1 (cm)	3 (cm)	5 (cm)	1 (cm)	3 (cm)	5 (cm)
$E(t_b)$%	0.23	0.56	0.61	0.02	0.02	0.26
MPSD	1776.38	58.56	73.52	51.84	73.65	114.89

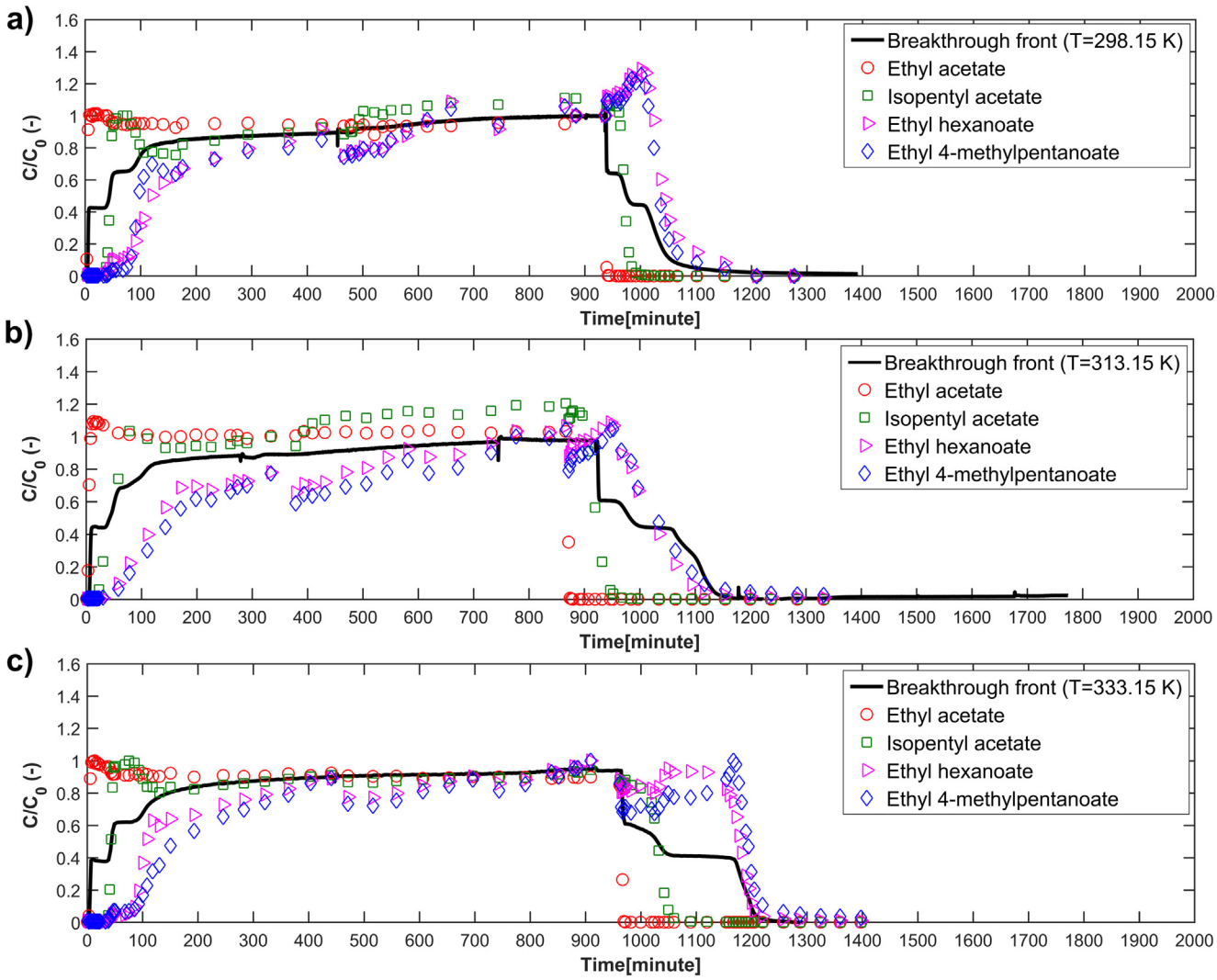

Fig. 3. Comparison of competitive breakthrough fronts with collected fractions for adsorption/elution of multi-component mixture of esters on a 1 cm Sepabeads SP20SS column prepared in 1% v/v ethanol; (a) T = 298.15 K (b) T = 313.15 K (c) T = 333.15 K.

plateau and the corresponding concentrations are measured in each sub-plateau for each component and also from fraction collection and offline analysis. The comparison of equilibrium binding capacity calculated based on competitive frontal analysis and integration of the breakthrough curves constructed through fraction collection and offline analysis are illustrated in Fig. 4, *part a* for adsorption on a 1 cm column packed with Sepabeads SP20SS resin and for the three tested temperatures. The calculated values for binding capacity for each ester present in the multi-component mixture reveal that, increase in temperature is not favorable for adsorption of the flavor-active esters since

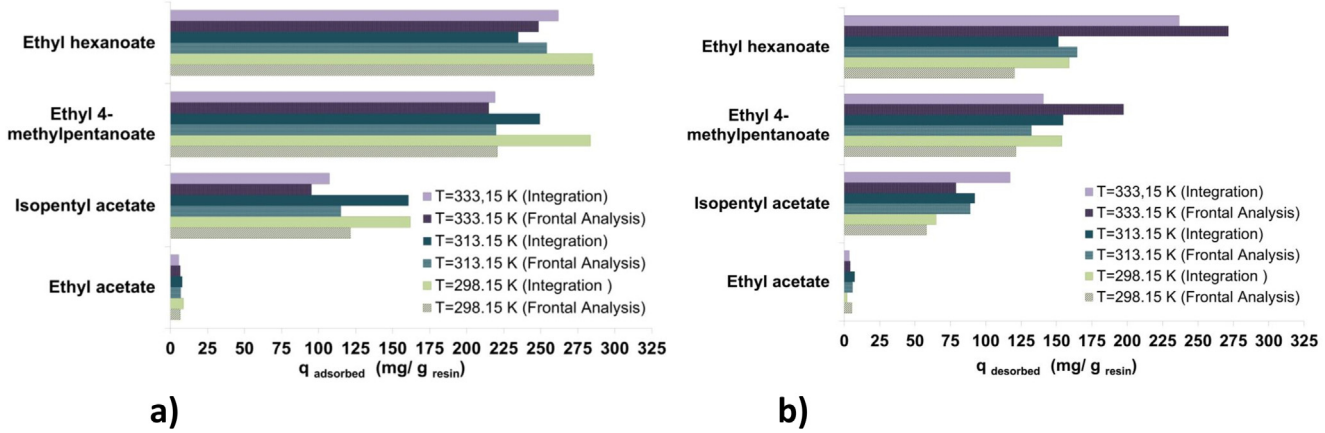

Fig. 4. Equilibrium binding capacity (adsorption) and mass eluted per gram of the packed resin from the column (elution) estimated at three tested temperatures and for the four esters, 1 cm Sepabeads SP20SS column, initial solution prepared in 1%v/v Ethanol; (a) Adsorption (b) Elution.

their adsorption is exothermic, which phenomena was also observed in our previous studies on single and multi-component adsorption, using batch uptake experimentation [8]. It can be clearly observed from Fig. 4, *part a*, that the more hydrophobic the tested ester is, the higher will be the value of q (equilibrium binding capacity), as the component has more affinity for binding to the resin surface. The difference caused in estimations based on competitive frontal analysis and the integration is due to the constructed breakthrough curves, which are obtained from offline analysis and experimental measurements, which has influence on the shape of the breakthrough curves and integrated areas.

The same procedure is applied for estimation of the amount eluted for each component from the column. The results are presented in Fig. 4, *part b*, where the calculated values based on competitive frontal analysis and integration are compared for each ester present in the mixture. Comparing the estimated values for the equilibrium binding capacity and the amount of mass, which is eluted from the resin, at various temperatures, we can conclude that, more components are released from the column and eluted at higher tested temperature, as almost between 63 and 100% of the adsorbed esters are recovered at 333.15 K. It is then followed by 313.15 K, in which 60–90% of the esters are eluted from the column. In comparison, lower recovery (40–80%) was achieved when elution was performed at lower temperature (298.15 K).

4.3.2. *Influence of ethanol concentration*

Influence of ethanol concentration on multi-component adsorption behavior of the major flavor-active esters of interest is investigated at temperature 333.15 K on a 1 cm column packed with Sepabeads

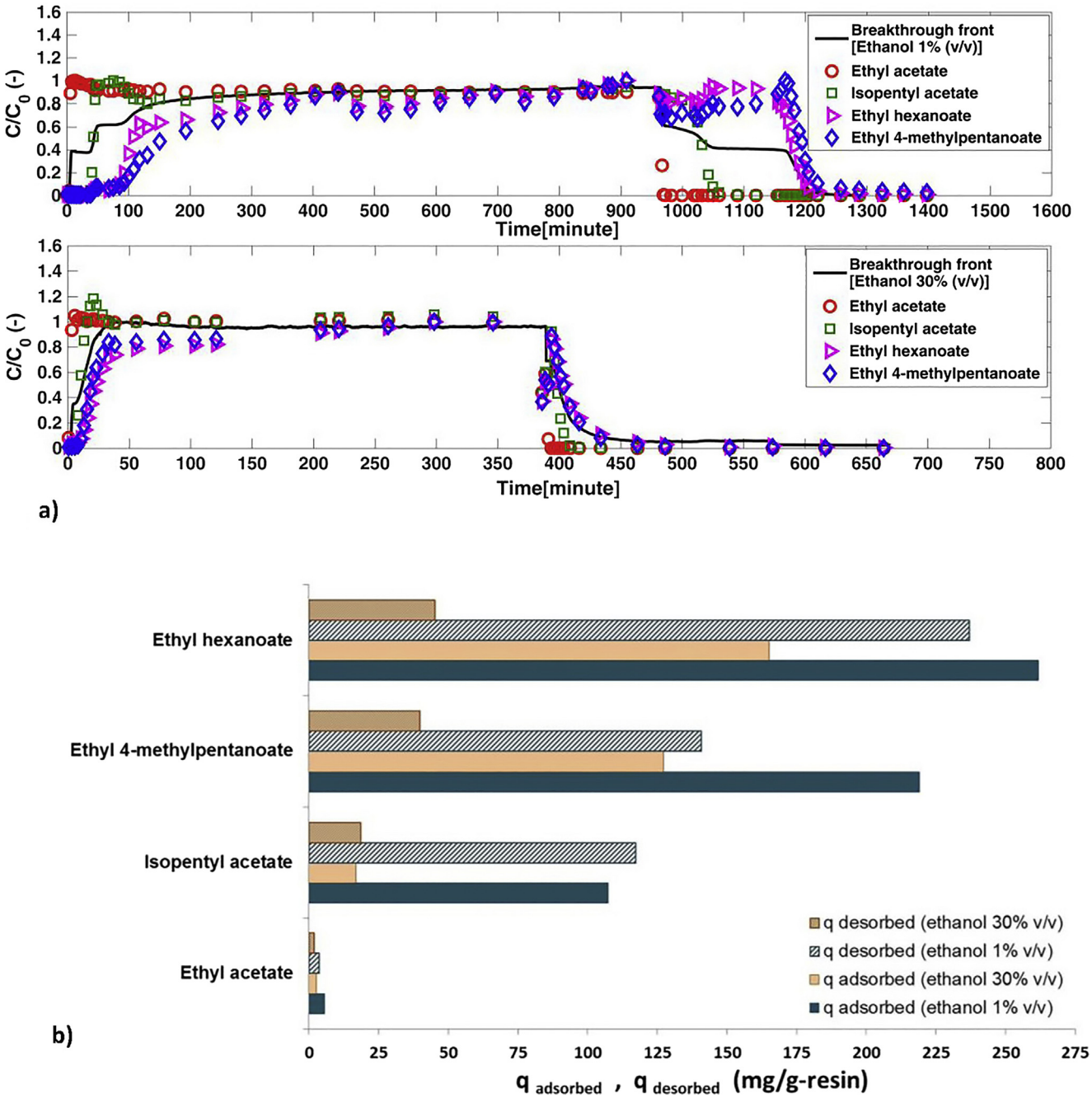

Fig. 5. Adsorption/elution of multi-component mixture of esters on a 1 cm Sepabeads SP20SS column at 333.15 K, tested at ethanol concentrations 1 and 30% v/v; (a) Competitive breakthrough fronts with collected fractions (b) Comparison of equilibrium binding capacity and the mass of the esters eluted from the column.

SP20SS, for initial samples prepared in 1, and 30% v/v co-solvent mixtures of ethanol/water. During the breakthrough analysis time, fractions are collected and analyzed with HS-GC. The comparison of the breakthrough fronts and the collected fractions is presented in Fig. 5, *part a*, As the competitive breakthrough front illustrates, at higher percentage of ethanol (i.e. 30% v/v), separate sub-plateaus cannot be observed for each ester present in the mixture and the breakthrough time is reduced to a great extent in comparison to the tested case with 1% (v/v) ethanol, therefore it makes it difficult to estimate the equilibrium binding capacity associated with each ester present in the mixture using the sub-plateaus as separate breakthrough curves are not detected.

For this reason the amount of equilibrium binding capacity is estimated based on the breakthrough curves, constructed from fraction collection and off-line analysis and compared with previously estimated equilibrium binding capacity calculated for adsorption/elution at 1% v/v ethanol and T = 333.15 K, presented also in Fig. 4. The comparison of the estimated equilibrium binding capacities is depicted in Fig. 5, *part b*. It can be concluded from Fig. 5 that increase in ethanol concentration from 1 to 30% v/v has influence on equilibrium binding capacity of esters, as lower equilibrium binding capacity is calculated for the condition when the ethanol concentration is 30% v/v in comparison to 1% v/v from integration of the breakthrough curves. Increase in the ethanol concentration in the mixture from 1 to 30% v/v lowers the activity coefficient of esters in the liquid phase, and as esters have less tendency to leave the aqueous phase, lower amount of esters is bound to the resin at higher ethanol concentrations.

4.4. Cyclic operation for adsorption/elution in a fixed-bed column

4.4.1. Adsorption/elution cycle for each tested resin

Multi-component competitive adsorption/elution behavior of the flavor-active esters, is simulated in Aspen Adsorption and breakthrough curves are obtained for one batch cycle for adsorption on both resins, (i.e. Sepabeads SP20SS and Amberlite XAD16N), for adsorption on a 1 cm column, at T = 333.15 K and solutions prepared in 30% (v/v) ethanol/water co-solvent mixture. In order to compare the influence of resin structure and properties on shape of the breakthrough curves and on breakthrough cycle time, the simulation results are compared for both resins, also explained by constructed breakthrough curves derived from fraction collection and offline analysis. One batch cycle is simulated through cycle organizer in Aspen Adsorption and the breakthrough time is considered the same as the time obtained from fraction collection and complete breakthrough for all the tested esters in the mixture. The comparison of the breakthrough curves together with the collected fractions is presented in Fig. 6, for adsorption on Sepabeads SP20SS and Amberlite XAD16N respectively.

It can be observed from Fig. 6, that the simulated breakthrough curves are able to predict the experimental breakthrough curves with higher accuracy for Amberlite XAD16N, and the stepwise breakthrough for ethyl hexanoate and ethyl 4-methylpentanoate and the slight overshoot observed for isopentyl acetate is not well-predicted by simulation for adsorption on Sepabeads SP20SS resin. Longer breakthrough time and mass transfer zone, is achieved for separation on XAD16N in comparison to SP20SS resin, as was also observed previously for single component adsorption of the flavor-active esters, illustrated in Figs. 1 and 2 due to larger particle size of XAD16N and smaller pore volume of this resin as discussed before. The estimated percent standard deviation between the simulated breakthrough curves and the experimental collected fractions, and the deviation between the experimental and simulated breakthrough times are reported in Table 3.

From presented values in Table 3, it can be concluded that simulated breakthrough curves are able to predict the multi-component separation for XAD16N with higher accuracy in comparison to SP20SS, as lower values for MPSD are estimated for XAD16N and due to the deviation of the model prediction from the experimental behavior observed for the two components ethyl acetate and Isopentyl acetate and the overshoot detected in experimental data due to displacement effects and competition of the flavor-active esters in the mixture for

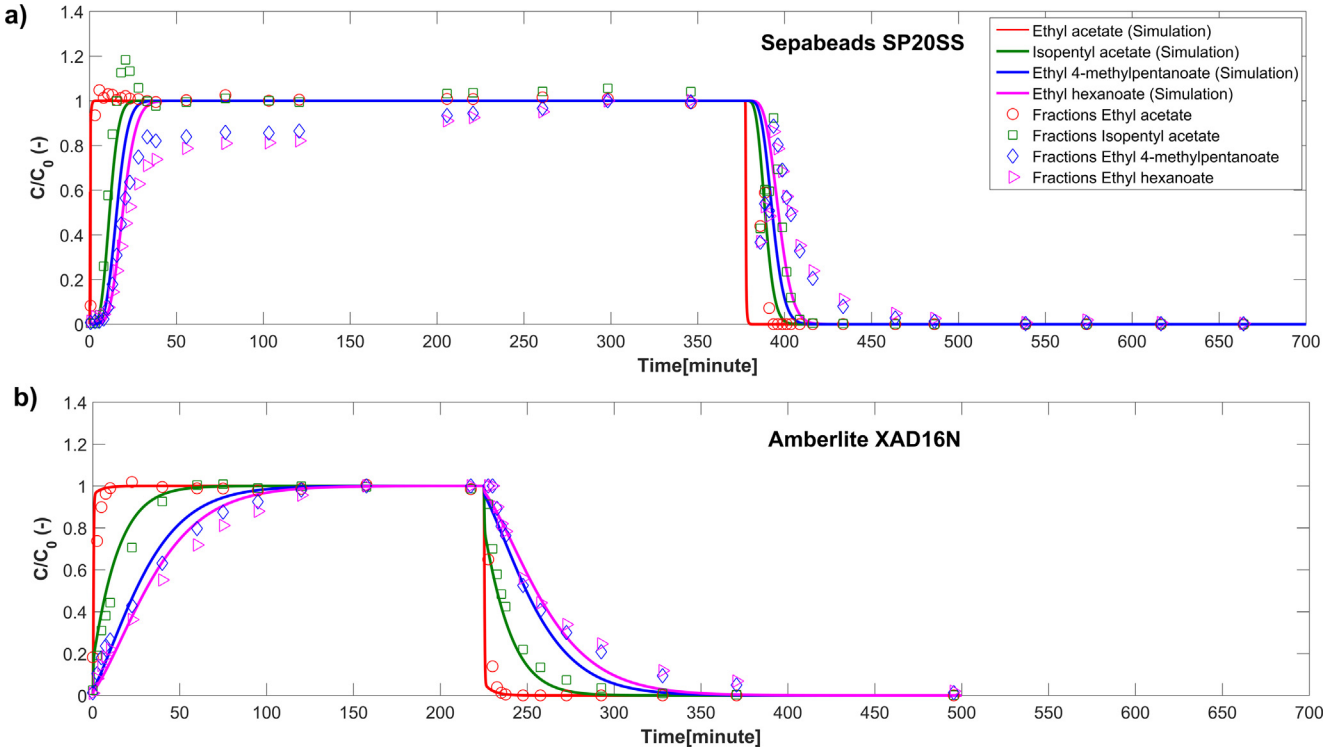

Fig. 6. Comparison of simulated breakthrough cycle and collected fractions for adsorption of multi-component mixture of esters (prepared in 30% ethanol) on a 1 cm column packed with (a) Sepabeads SP20SS b) Amberlite XAD16N resin; (Adsorption at T = 333.15 K).

Table 3
Estimated errors for breakthrough times and percent standard deviation between simulated breakthrough curves and experimental breakthrough curves obtained from fraction collection; Adsorption at 333.15 K and 30% v/v Ethanol.

	Sepabeads SP20SS		Amberlite XAD16N	
	$E(t_b)$%	MPSD	$E(t_b)$%	MPSD
Ethyl acetate	−0.17	308.17	1.22	42.44
Isopentyl acetate		482.08		99.99
Ethyl 4-methylpentanoate		76.78		49.48
Ethyl hexanoate		87.36		48.64

adsorption, the simulated breakthrough curves predicted the adsorption behavior for these two components with less accuracy in comparison to the other tested components.

4.4.2. Influence of temperature and ethanol concentration on adsorption/elution cycle on Sepabeads SP20SS

To investigate the influence of temperature and ethanol concentration on one adsorption/elution cycle of flavor-active esters, adsorption/elution breakthrough behavior is simulated for a column packed with Sepabeads SP20SS resin as is explained in Appendix E, and simulated breakthrough cycles are compared, illustrated in Fig. E.1.

4.4.3. Cyclic operation in a larger scale column

Studying the influence of temperature and ethanol concentration on adsorption/elution behavior of flavor-active esters in a lab-scale column, gives us an insight about the possibility of their separation and important parameters which are required to be considered, when tests are going to be performed in a larger scale column. With the conclusions obtained from experimental tests, a similar condition is considered for simulation of the breakthrough behavior and cyclic operation for a larger scale column. The column length of 2 m and internal column diameter of 0.08 m, are selected as typical column dimensions [34], in order to test the model based approach for prediction of breakthrough behavior for separation of flavor-active esters. Higher flow-rate, 300 L/hr is considered for each batch cycle. The simulation is performed again for the case with initial solution of esters prepared in 1% v/v ethanol/water co-solvent mixture and adsorption at T = 298.15 K. Two batch cycle operations are programed using cycle organizer in Aspen Adsorption. Two different scenarios are considered for the simulation. The first scenario is simulated based on recovery and separation of ethyl acetate, the main flavor-active ester present in the beer matrix, and this ester is considered as the limiting ester in the mixture (column loading until breakthrough for ethyl acetate is achieved). The second scenario is simulated based on removal and complete adsorption of all of the flavor-active esters present in the mixture. In the initial step in each simulated cycle, the adsorption of flavor-active esters takes place at T = 298.15 K, it is then followed by elution step, which is performed with 1% v/v ethanol solution and direct temperature increase from 298.15 K to 380.15 K, as a temperature increase will aid the elution step and release of the high hydrophobic components of the column. Temperature of 380.15 K is selected as maximum allowable temperature, due to the thermo-stability of the resin and flavor-active esters at higher temperatures. After the elution step, the column is washed with water at high temperature (380 K) to

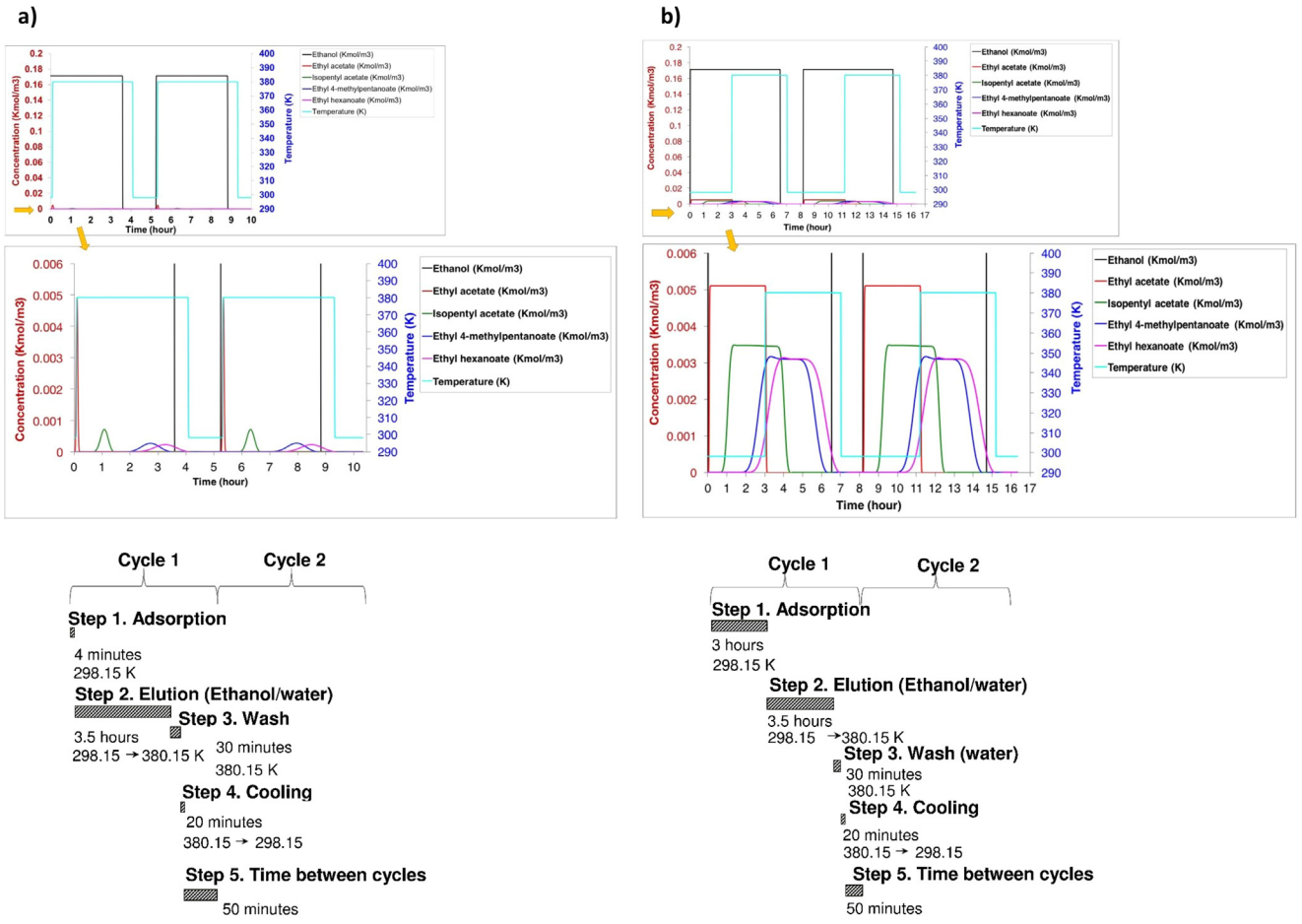

Fig. 7. Cyclic operation for two batch cycles, column packed with Sepabeads SP20SS resin (L = 2 m, D = 0.08 m); (a) Adsorption and recovery of ethyl acetate (b) Adsorption and recovery of four esters.

elute the traces of ethanol for 30 min and cooled down during 20 min to the initial temperature of 298.15 K. The second cycle will start within 50 min with the same condition defined for the initial cycle. The result of the simulation for two batch cycles is shown in Fig. 7, *part a*, for the first scenario, removal of ethyl acetate, and in Fig. 7, *part b*, for complete removal of all of the flavor-active esters from the initial feed stream. The considered conditions for each step are presented for one batch cyclic operation in Fig. 7.

The selected operating conditions for the simulation together with explanation of the calculations for percentages of recovery are explained in Appendix E, Table E1. For the first scenario, higher recovery of ethyl acetate can be achieved in comparison to the other tested esters, since after the breakthrough time for this ester as the limiting component, the elution step starts and specifically the two esters with the highest hydrophobicity, do not have sufficient time for adsorption. In the second scenario, the percentage of ethyl acetate which is recovered (% c/a) is less in comparison to the other esters, since some amount of this ester component is lost during the loading time until the breakthrough point for the last hydrophobic ester is achieved and higher percentage of the last hydrophobic esters, i.e. ethyl 4-methylpentanoate, and ethyl hexanoate is recovered. For the first scenario, 1.2 m^3 of the feed stream can be processed during approximately 4 h considered for adsorption, elution, and washing steps, while in the second scenario, 2.1 m^3 of the feed stream is processed within 7 h for the same steps as scenario 1. Change in temperature of the adsorbent during each step and for the two simulated scenarios is not significant and maximum temperature difference for the adsorbent between column inlet and column outlet, is observed as 0.002°K, for scenario 1, and 0.03°K for scenario 2, during the temperature increase for the mobile phase from 298.15 to 380.15 K in the elution step. The condition considered for simulation here, is based on the tested condition for the lab-scale column. Similar condition is considered for adsorption and elution steps in a larger scale column to predict the breakthrough behavior, percentage of recovery, and batch operation time required for each cycle. In real process condition, the presence of other flavor and non-flavor-active components, besides CO_2 which is present in the process streams, will influence the adsorption behavior of esters, and for consideration of the adsorption step for removal of flavor-active esters or their fractionation, the influence of other components, should be considered on their competitive adsorption behaviour and performing an economic optimization step is necessary to determine the minimized column volume in order to maximize the production rate.

5. Conclusions

Competitive frontal analysis method combined with fraction collection was able to predict the binding capacity for flavor-active esters and to measure the equilibrium concentrations in intermediate subplateaus of the breakthrough front. Increase in temperature was not favourable for adsorption of esters on SP20SS resin; however, temperature increase enhanced their elution from the column. Increase in ethanol concentration reduced the breakthrough time for adsorption to a great extent. The simulated breakthrough behavior for the tested esters, revealed a shorter cycle time and breakthrough curves with a higher slope for SP20SS in comparison to XAD16N, which can be explained by smaller particle size and enhanced mass transfer characteristics of this resin. Cycle time for simulated adsorption/elution step for a column packed with this resin, showed a decrease (approximately five times) with increase in temperature and ethanol concentration. Simulated breakthrough curves for multi-component separation of esters showed higher accuracy and agreement with the experimental breakthrough curves constructed through fraction collection for XAD16N in comparison to SP20SS. Breakthrough behavior and cyclic operation simulated for a larger scale column, showed recovery for ethyl acetate and its separation from other flavor-active esters (scenario 1), and complete separation of esters (scenario 2). In order to be able to perform a more detailed simulation for prediction of breakthrough behavior, the influence of other components in the mixture on competitive adsorption of esters and the influence of process conditions and parameters needs to be further investigated.

Acknowledgements

This research work took place in the framework of ISPT (Institute of Sustainable Process Technology), under the grant number FO-10-05. We would like to acknowledge ISPT for its support and thank Heineken Supply Chain for valuable comments.

Appendix A. Physical properties of adsorbents and tested ester components

(See Tables A1–A3).

Table A1
Physical properties of tested adsorbents.

Resin	Matrix	Particle size (μm)	Pore volume (ml/g)	Mean pore size (Å)	Surface area (m^2/g)	Dry density (vs. wet) (g/ml)
Sepabeads SP20SS	Styrene-divinylbenzene	50–100	1.01	260	500	(1.3)
Amberlite XAD16N	Styrene-divinylbenzene	560–710	0.55	200	800	1.08 (1.02)

Table A2
Physical properties of the tested flavor-active esters.

Component	Molecular structure	Molar mass (g.mol^{-1})	Log P	Solubility (mol.L^{-1})	Solvent accessible surface area (Å)^2	Flavor description
Ethyl acetate	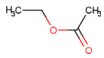	88.106	0.28	0.03	287.33	Solvent-like, nail polish
Isopentyl acetate	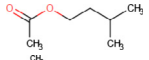	130.187	1.53	−1.41	375.79	Banana, Pear drop
Ethyl 4-methylpentanoate	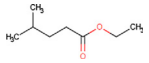	144.214	2.16	−1.92	412.57	apple
Ethyl hexanoate	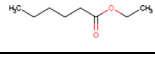	144.214	2.31	−1.99	438.56	apple

Table A3
Heat of adsorption for flavor-active esters.

	Heat of adsorption (ΔH) (KJ.mol^{-1})	
	Sepabeads SP20SS	Amberlite XAD16N
Ethyl acetate	−13.64	−12.57
Isopentyl acetate	−25.05	−20.26
Ethyl 4-methylpentanoate	−28.12	−21.07
Ethyl hexanoate	−30.66	−31.13

Appendix B. Expression of apparent dispersion coefficient (D_{app})

For equilibrium dispersive model, Eqs. (B.1) and (B.2) represent the relation between $\widetilde{D}_{app,i}$ and apparent dispersion coefficient (D_{app}), axial dispersion coefficient (D_{ax}) and effective mass transfer coefficient (k_{eff}) [26].

$$\widetilde{D}_{app,i} = \frac{u}{u_{int}} D_{app,i} \tag{B.1}$$

$$D_{app} = D_{ax} + \left(\frac{\widetilde{k}'}{1+\widetilde{k}'}\right)^2 \frac{\varepsilon}{1-\varepsilon} \frac{r_p}{3} \frac{{u_{int}}^2}{k_{eff}} \tag{B.2}$$

Parameter D_{ax}, expresses the axial dispersion which sums the contribution of axial molecular diffusion and eddy diffusion [33,46]. $\widetilde{k}'$ has relation with the retention factor of the component of interest between the mobile and stationary phase (k') according to Eq. (B.3) [26]. $\widetilde{k}'$ can be calculated from the difference between retention time of component i ($t_{R,i}$) and the dead time of the column for total liquid holdup (t_0), divided by t_0 [26]. k_{eff} is the effective mass transfer coefficient, which can be estimated from film mass transfer coefficient and pore diffusion [26].

$$\widetilde{k}' = \frac{\varepsilon_T}{\varepsilon}(1+k') - 1 \tag{B.3}$$

Appendix C. Assumptions and conditions for simulation in Aspen adsorption

The information related to configuration of the adsorbent bed and the equations for each layer of adsorbent are adjusted in the configuration form, [50,57] Mixed Differencing Scheme (MDS) with 29 nodes is used as the discretization method, with the advantage of having precision and more stability [50,57]. As the assumption for material balance, convection with estimated dispersion is considered for the simulation and the dispersion coefficient is estimated as explained in Section 2.2.2.1. Varying velocity is assumed inside the column and pressure drop is estimated based on Kozeny-Carman relation. For the kinetic model assumption, linear lumped resistance is considered for the simulation. As the isotherm model, multi-component Langmuir model, presented in Eq. (3), is considered and the Langmuir parameters are obtained from batch uptake experimentation, based on previous work [8]. Energy balance is assumed as non-isothermal with conduction in fluid and solid phase. Heat of adsorption for each tested ester, acquired from our previous study [8] is used for the simulation of non-isothermal condition. Heat transfer to the environment is considered as adiabatic and the last term in Eq. (6) is neglected. Cyclic operation is simulated with step control, using cycle organizer. Time driven steps are simulated for adsorption, elution, washing, and cooling steps and required cyclic operation time for each batch cycle is obtained for the two different simulated scenarios.

Appendix D. Estimation of equilibrium binding capacity based on competitive frontal analysis

A sample of a breakthrough front is shown in Fig. D.1 for a three-component mixture.

In the left figure, breakthrough front for adsorption is depicted. In the first breakthrough curve, the least binding compound will be detected with the breakthrough (BT) volume of V_{a1} (ml). The second component with stronger hydrophobicity will be detected in the second sub-plateau, followed by the third compound with the highest hydrophobicity, which will be present in the third breakthrough front, until the concentration in the outlet reaches the feed concentration. The amount of analyte adsorbed on the column can be calculated for each component, according to Eqs. (D.1)–(D.3).

a. For adsorption of the first component

$$q_{1,ads} = \frac{(V_{a3}-V_h)C_1^{Feed} - (V_{a3}-V_{a2})C_{1.ads}^3 - (V_{a2}-V_{a1})C_{1,ads}^2}{m_{resin}} \tag{D.1}$$

b. For adsorption of the second component

$$q_{2,ads} = \frac{(V_{a3}-V_h)C_2^{Feed} - (V_{a3}-V_{a2})C_{2,ads}^3}{m_{resin}} \tag{D.2}$$

c. For adsorption of the third component

$$q_{3,ads} = \frac{(V_{a3}-V_h)C_3^{Feed}}{m_{resin}} \tag{D.3}$$

where V_{a1}, V_{a2}, and V_{a3} (ml) are breakthrough volumes for adsorption of the first, second, and the third components respectively. $C_{1,ads}{}^3$ and $C_{2,ads}{}^3$

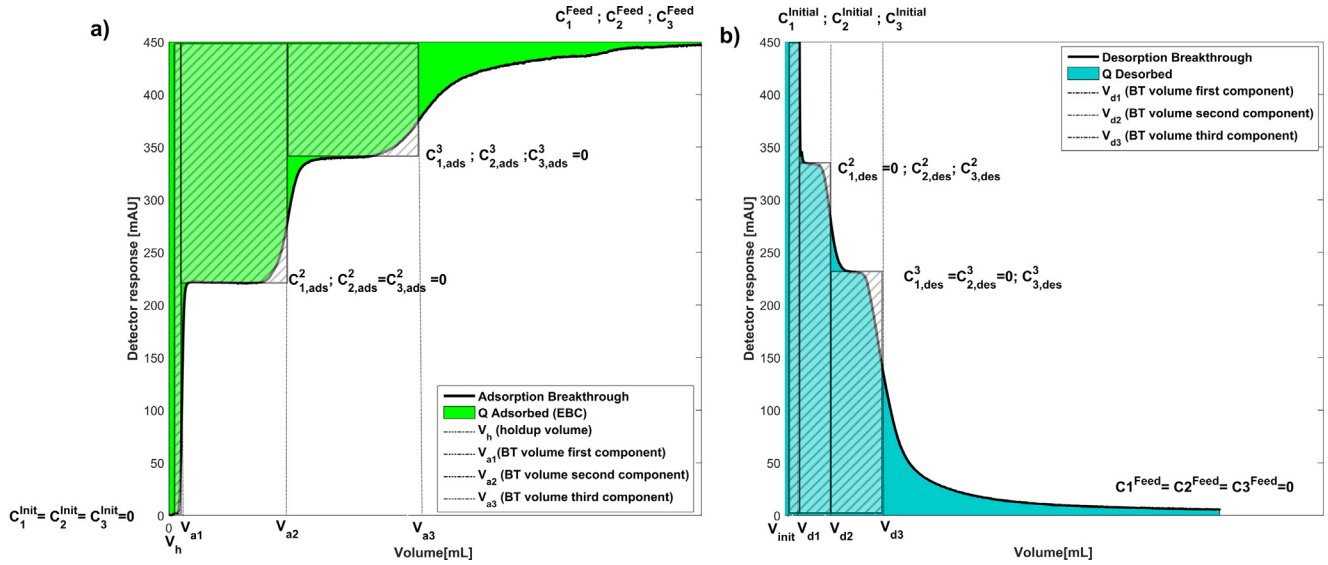

Fig. D1. Stepwise breakthrough fronts for adsorption and desorption of a ternary mixture; (a) Adsorption breakthrough front (b) Desorption breakthrough front.

(mg/ml) are the concentrations corresponding to the first and second components in the second plateau and $C_{1,ads}{}^2$ is the concentration of the first component in the first breakthrough front. m $_{resin}$ is the mass of the packed column (g), and $q_{1,ads}$, $q_{2,ads}$, and $q_{3,ads}$ are equilibrium binding capacities for the first, second, and the third component (mg/g $_{resin}$). The mass of each component desorbed from the resin can be estimated according to Eqs. (D.4)–(D.6), assuming symmetrical frontal sub-plateaus as is depicted in Fig. D.1, *part b*, from desorption breakthrough frontal curve.

d. For desorption of the first component

$$q_{1,des} = \frac{(V_{d1} - V_{init})C_1^{init}}{m_{resin}} \tag{D.4}$$

e. For desorption of the second component

$$q_{2,des} = \frac{(V_{d1} - V_{init})C_2^{init} + (V_{d2} - V_{d1})C_{2,des}^2}{m_{resin}} \tag{D.5}$$

f. For desorption of the third component

$$q_{3,des} = \frac{(V_{d1} - V_{init})C_3^{init} + (V_{d2} - V_{d1})C_{3,des}^2 + (V_{d3} - V_{d2})C_{3,des}^3}{m_{resin}} \tag{D.6}$$

where V_{d1}, V_{d2}, and V_{d3} (ml) are breakthrough volumes for desorption of the first, second, and the third components respectively. $C_{3,des}{}^2$ and $C_{2,des}{}^2$ (mg/ml) are the concentrations corresponding to the third and second components in the second plateau and $C_{3,des}{}^3$ is the concentration of the third component in the last sub-plateau of the breakthrough front. $q_{1,des}$, $q_{2,des}$, and $q_{3,des}$ are masses for the first, second, and the third component (mg/g $_{resin}$) eluted from the column.

Appendix E. Batch adsorption/elution cycle for Sepabeads SP20SS column

For adsorption on 1 cm Sepabeads SP20SS column and for two tested cases (a) Solution of esters prepared in 1% v/v ethanol solution and adsorption at T = 298.15 K, and (b) Solution of esters prepared in 30% v/v ethanol solution and adsorption at T = 333.15 K, the simulated breakthrough cycles for the two cases are compared in Fig. E.1.

It can be detected from Fig. E.1 that the cycle time reduces almost to one fifth, when adsorption takes place at higher temperature and adsorption/elution is performed with 30% v/v of ethanol solution. The observed decrease in cycle time can be explained by influence of temperature on adsorption and elution step, which is discussed in detail in Section 4.3. Also influence of increase in ethanol percentage from 1 to 30% v/v observed as considerable on binding capacity of esters as discussed in Section 4.3.2, and performing the experiment at both high concentration of ethanol and at high temperature, leads to less binding of ester components and enhanced elution characteristics.

For the performed simulation for a larger scale column packed with the same resin, the column operating condition together with the percentage of recovery for each tested ester during each programed cycle and for each scenario is presented in Table E1.

In order to calculate the percentage of recovery for each ester component, the number of moles eluted after the adsorption step are calculated through integrating the area under the breakthrough curve for the similar time defined for adsorption step in the simulation. The percentage of each ester component recovered after the elution step is then calculated as the ratio of the number of moles eluted to the initial number of moles of the ester in the feed stream. The number of moles adsorbed for each tested flavor-active ester are calculated based on Eq. (E.1).

$$Number\ of\ moles\ adsorbed = \int_0^{t_{BT,i}+t_{step1}} (F \times C_{i,out} \times dt) \tag{E.1}$$

where $t_{BT,i}$ represents the breakthrough time for each ester component (hr). The productivity for each simulated scenario is reported as the volume of

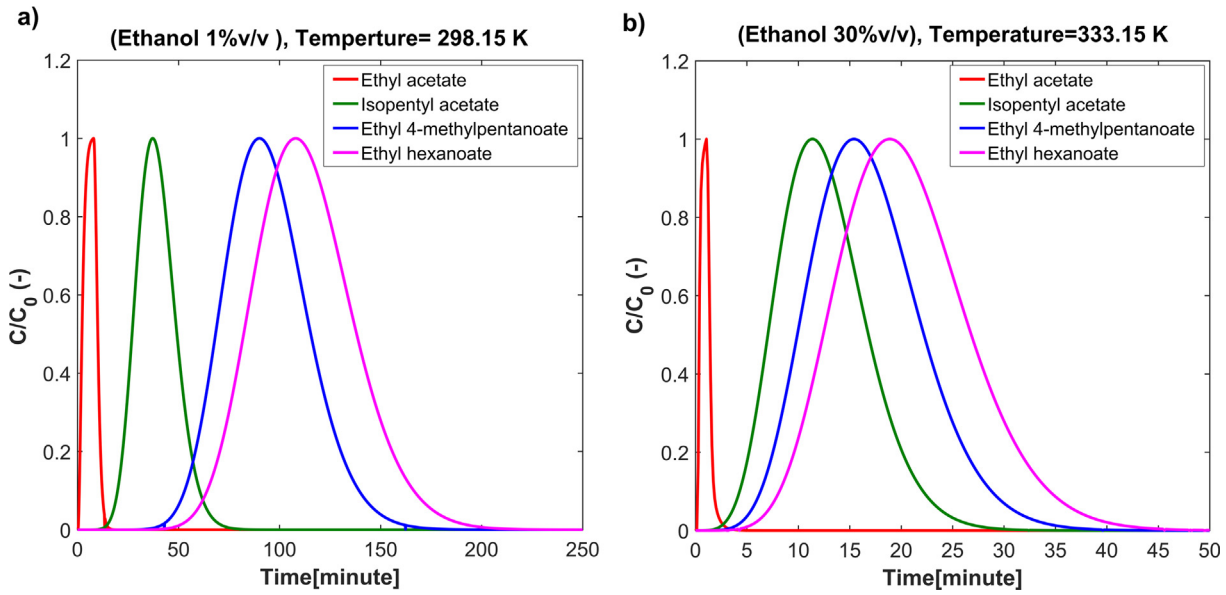

Fig. E1. Comparison of adsorption/elution cycle for adsorption on a 1 cm column packed with Sepabeads SP20SS resin and two cases; (a) Solution of esters prepared in 1% v/v Ethanol and adsorption at T = 298.15 K, (b) Solution prepared in 30% v/v Ethanol and adsorption at T = 333.15 K.

Table E1
Column operating condition and percentage of recovery for each ester in the product stream during each programed cycle and for each simulated scenario.

Column operating condition				
Column length (m)	2			
Column diameter (m)	0.08			
F (m^3/hr)	0.3			
T (adsorption) (K)	298.15			
T (elution) (K)	298.15 , direct increase to 380.15			
	Scenario 1. Separation of ethyl acetate			
Component	*Ethyl acetate*	*Isopentyl acetate*	*Ethyl 4-methylpentanoate*	*Ethyl hexanoate*
$C_{i,\ Feed}$ (mol/m^3)	5.11	3.46	3.12	3.12
Number of moles loaded (a) (mol)	0.10	0.07	0.62	0.62
Number of moles adsorbed (b) (mol)	0.037	0.025	0.009	0.004
Number of moles eluted (c) (mol)	0.037	0.024	0.009	0.004
% c/b	100.33	94.29	100.75	100.38
% c/a	37.06	34.58	15.83	4.30
Productivity (m^3)	1.20			
	Scenario 2. Separation of all esters			
Number of moles loaded (a) (mol)	4.60	3.11	2.81	2.81
Number of moles adsorbed (b) (mol)	0.090	1.080	2.489	2.459
Number of moles eluted (c) (mol)	0.091	1.080	1.979	2.009
% c/b	100.67	100	79.52	81.71
% c/a	1.97	34.68	70.51	71.58
Productivity (m^3)	2.09			

feed stream (m^3) that can be processed during the considered cycle time (time for loading, elution, and washing step), shown Table E1 for each scenario.

Appendix F. Supplementary material

Supplementary data associated with this article can be found, in the online version, at https://doi.org/10.1016/j.seppur.2018.05.008.

References

[1] S.S.H. Rizvi, Separation, Extraction and Concentration Processes in the Food, Beverage and Neutraceutical Industries, Woodhead Pub, Oxford, 2010.
[2] P. Schoenmakers, Chromatography in industry, Annu. Rev. Anal. Chem. 2 (2009) 333–357.
[3] S. Fanali, P.R. Haddad, C. Poole, P. Schoenmakers, D.K. Lioyd, Liquid Chromatography, Elsevier Inc., 2013.
[4] A.O. Olaniran, L. Hiralal, M.P. Mokoena, B. Pillay, Flavor-active volatile compounds in beer: production, regulation and control, J. Inst. Brew. 123 (2016) 13–23.
[5] E.J. Pires, J.A. Teixeira, T. Branyik, A.A. Vicente, Yeast: the soul of beer's aroma-a review of flavour-active esters and higher alcohols produced by the brewing yeast, Appl. Microbiol. Biotechnol. 98 (2014) 1937–1949.
[6] D. Saison, D.P. De Schutter, B. Uyttenhove, F. Delvaux, F.R. Delvaux, Contribution of staling compounds to the aged flavour of lager beer by studying their flavour

thresholds, Food Chem. 114 (2009) 1206–1215.
[7] L. Hiralal, A.O. Olaniran, B. Pillay, Aroma-active profile of ale beer produced under different fermentation and nutritional conditions, J. Biosci. Bioeng. 117 (2014) 57–64.
[8] S. Saffarionpour, S.Y.S. Tam, L.A. Van der Wielen, E. Brouwer, M. Ottens, Influence of ethanol and temperature on adsorption of flavor-active esters on hydrophobic resins, Sep. Purif. Technol . (2018).
[9] G.A.F. Harrison, The flavour of beer – a review, J. Inst. Brew. 76 (1970) 486–495.
[10] D.A. Gee, W.F. Ramirez, A flavour model for beer fermentation, J. Inst. Brew. 100 (1994) 321–329.
[11] A. Andrzejewska, K. Kaczmarski, G. Guiochon, Theoretical study of the pulse method, frontal analysis, and frontal analysis by characteristic points for the determination of single component adsorption isotherms, J. Chromatogr. A 1216 (2009) 1067–1083.
[12] G. Guiochon, A. Felinger, D.G. Shirazi, A.M. Katti, Fundamentals of preparative and nonlinear chromatography second ed., Elsevier Inc., San Diego, CA,USA, 2006.
[13] F. Kamarei, F. Gritti, G. Guiochon, J. Burchell, Accurate measurements of frontal analysis for the determination of adsorption isotherms in supercritical fluid chromatography, J. Chromatogr. A 1329 (2014) 71–77.
[14] S.C. Jacobson, A. Felinger, G. Guiochon, Optimizing the sample size and the reduced velocity to achieve maximum production rates of enantiomers, Biotechnol. Prog. (1992) 533–539.
[15] Z. Ma, G. Guiochon, Comparison between the hydrograph transform method and frontal chromatography for the measurement of binary competitive adsorption isotherms, J. Chromatogr. A 603 (1992) 13–25.
[16] S. Sun, G. Yang, H. Sun, D. Eang, H. Liu, Determination and comparison of competitive isotherms by rectangular pulse method and frontal velocity analysis method, J. Chromatogr. A 918 (2001) 13–23.
[17] S. Saffarionpour, D. Mendez Sevillano, L.A.M. Van der Wielen, T.R. Noordman, E. Brouwer, M. Ottens, Selective adsorption of flavor-active components on hydrophobic resins, J. Chromatogr. A 1476 (2016) 25–34.
[18] M.L. Soto, E. Conde, N. Gonzales-Lopez, M.J. Conde, A. Moure, J. Sineiro, E. Falque, H. Dominguez, M.J. Nunez, J.C. Parajo, Recovery and concentration of antioxidants from winery wastes, Molecules 17 (2012) 3008–3024.
[19] M.L. Soto, A. Moure, H. dominguez, J.C. Parajo, Batch and fixed bed column studies on phenolic adsorption from wine vinasses by polymeric resins, J. Food Eng. 209 (2017) 52–60.
[20] E.M. Silva, D.R. Pompeu, Y. Larondelle, H. Rogez, Optimization of the adsorption of polyphenols from Inga edulis leaves on macroporous resins using an experimental design methodology, Sep. Purif. Technol. 53 (2007) 274–280.
[21] Sigma-Aldrich, accessed in, 2017. < https://www.sigmaaldrich.com/nederland.html?gclid=EAIaIQobChMItZG3quyM2wIVVBobCh3PAAELEAAYASAAEgK0tfD_BwE>.
[22] P.R. Kasten, L. Lapidus, N.R. Amundson, Mathematics of adsorption in beds.V.effect of intra-particle diffusion in flow systems in fixed beds, J. Phys. Chem. 56 (1952) 683–688.
[23] K. Horvath, J.N. Fairchild, K. Kaczmarski, G. Guichon, Martin-Synge algorithm for the solution of equilibrium-dispersive model of liquid chromatography, J. Chromatogr. A 1217 (2010) 8127–8135.
[24] S. Golshan-Shirazi, G. Guiochon, Modeling of preparative liquid chromatography, J. Chromatogr. A 658 (1994) 149–171.
[25] B.K. Nfor, D.S. Zuluaga, P.J.T. Verheijen, P.D.E.M. Verhaert, L.A.M. Van der Wielen, M. Ottens, Model-based rational strategy for chromatographic resin selection, Biotechnol. Prog. 27 (2011).
[26] M. Michel, A. Epping, A. Jupke, Modeling and determination of model parameters, in: H. Schmidt-Traub (Ed.), Preparative Chromatography, WILEY-VCH Verlag GmbH & Co., Weinheim, 2005.
[27] G. Guiochon, Preparative liquid chromatography, J. Chromatogr. A 965 (2002) 129–161.
[28] L. Yanxu, C. Jiangyo, S. Yinghuang, Adsorption of multicomponent volatile organic compounds on semi-coke, Carbon 46 (2008) 858–863.
[29] G. Storti, M. Masi, S. Carra, M. Morbidelli, Optimal design of multicomponent countercurrent adsorption separation processes involving nonlinear equilibria, Chem. Eng. Sci. 44 (1989) 1329–1345.
[30] M. Mazzotti, G. Storti, M. Morbidelli, Shock layer analysis in multicomponent chromatography and countercurrent adsorption, Chem. Eng. Sci. 49 (1994) 1337–1355.
[31] M. Kaspereit, A. Seidel-Morgenstern, Process concepts in preparative chromatography, in: S. Fanali, P.R. Haddad, C. Poole, P. Schoenmakers, D.K. Lioyd (Eds.) Liquid Chromatography, Fundamentals and Instrumentation, Elsevier Inc., 2013.
[32] S. Qamar, S. Perveen, A. Seidel-Morgenstern, Numerical approximation of nonlinear and non-equilibrium two-dimensional model of chromatography, Comput. Chem. Eng. 94 (2016) 411–427.
[33] O. Lisec, P. Hugo, A. Seidel-Morgenstern, Frontal analysis method to determine competitive adsorption isotherms, J. Chromatogr. A 908 (2001) 19–34.
[34] D.M. Ruthven, Principles of adsorption and adsorption processes, John Wiley & Sons Inc., USA, 1984.
[35] P.C. Carman, Fluid flow through granular beds, Trans. Inst. Chem. Eng. 15 (1937) 150–167.
[36] B.R. Corrochano, J.R. Melrose, A.C. Bentley, P.J. Fryer, S. Bakalis, A new methodology to estimate the steady-state permeability of roast and ground coffee in packed beds, J. Food Eng. 150 (2015) 106–116.
[37] J. Kozeny, Capillary motion of water in soils, Sitzungsberichte der Akademie der Wissenschaften in Wien, Mathematisch-Naturwissenschaftliche Klasse, Sitzb Akad Wiss 136 (1927) 271–306.
[38] I.F. MacDonald, M.S. El-Sayed, K. Mow, F.A.L. Dullien, Flow through porous media-the Ergun equation revisited, Ind. Eng. Chem. Fundam. 18 (1979) 199–208.
[39] G.D. Scott, Packing of spheres: packing of equal spheres, Nature 188 (1960) 908–909.
[40] X. Lin, Q. Huang, G. Qi, S. Shi, L. Xiong, C. Huang, X. Chen, H. Li, X. Chen, Estimation of fixed-bed column parameters and mathematical modeling of breakthrough behaviors for adsorption of levulinic acid from aqueous solution using SY-01 resin, Sep. Purif. Technol. 174 (2017) 222–231.
[41] E.J. Wilson, C.J. Geankoplis, Liquid mass transfer at very low Reynolds numbers in packed beds, Ind. Eng. Chem. Fundam. 5 (1966) 9–14.
[42] C.R. Wilke, P. Chang, Correlation of diffusion coefficients in dilute solutions, AICHE J. 1 (1955) 264–270.
[43] C.W. Mohr, R.D. Vogt, O. Royset, T. Andersen, N.A. Parekh, An in-depth assessment into simultaneous monitoring of dissolved reactive phosphorus (DRP) and low-molecular-weight organic phosphorus (LMWOP) in aquatic environments using diffusive gradients in thin films (DGT), Environ. Sci-Proc. Imp. 17 (2015) 711–727.
[44] < https://www.chemaxon.com/>, in, 28 June, 2017.
[45] G. Carta, A. Jungbauer, Protein Chromatography: Process Development and Scale-up, Wiley-VCH Verlag GmbH & Co., Weinheim, 2010.
[46] A. Jungbauer, Insights into the chromatography of proteins provided by mathematical modeling, Curr. Opin. Biotech. 7 (1996) 210–218.
[47] A. Susanto, T. Hermann, E. Von Lieres, J. Hubbuch, Investigation of pore diffusion hindrance of monoclonal antibody in hydrophobic interaction chromatography using confocal laser scanning microscopy, J. Chromatogr. A 1149 (2007) 178–188.
[48] I. Quiñones, J.C. Ford, G. Guiochon, Multisolute adsorption equilibria in a reversed-phase liquid chromatography system, Chem. Eng. Sci. 55 (2000) 909–929.
[49] J.M. Reck, T.M. Pabst, A.K. Hunter, G. Carta, Separation of antibody monomer-dimer mixtures by frontal analysis, J. Chromatogr. A 1500 (2017) 96–104.
[50] E.H. Slaats, W. Markovski, J. Fekete, H. Poppe, Distribution equilibria of solvent components in reversed-phase liquid chromatographic columns and relationship with the mobile phase volume, J. Chromatogr. 207 (1981) 299–323.
[51] S. Sun, G. Yang, H. Sun, D. Wang, H. Liu, Determination and comparison of competitive isotherms by rectangular pulse method and frontal velocity analysis method, J. Chromatogr. A 918 (2001) 13–23.
[52] J.A. Vente, H. Bosch, A.B. de Haan, P.J.T. Bussmann, Evaluation of sugar sorption isotherm measurement by frontal analysis under industrial processing conditions, J. Chromatogr. A 1066 (2005) 71–79.
[53] D.W. Marquardt, An algorithm for least-squares estimation of nonlinear parameters, J. Soc. Ind. Appl. Math. 11 (1963) 431–441.
[54] V.C. Srivastana, B. Prasad, I.M. Mishra, I.D. Mall, M.M. Swamy, Prediction of breakthrough curves for sorptive removal of phenol by bagasse fly ash packed bed, Ind. Eng. Chem. Res. 47 (2008) 1603–1613.
[55] M.B. Kirkham, Structure and properties of water, in: Principles of soil and plant water relations, Academic Press, 2014.
[56] R. Hahn, R. Schleger, A. Jungbauer, Comparison of protein A affinity sorbents, J. Chromatogr. B-Anal. Technol. Biomed. Life Sci. 790 (2003) 35–51.
[57] M. Peighambarzadeh, M. Bohlool, Adsorption process and its simulation with ASPEN ADSIM, third ed., Andishehsara, Tehran, Iran, 2015.